

# TDQMS CW - The Schumann-Runge Band of the $^{16}\text{O}_2$ spectrum

Joe Hart - CID 01852112

word count: 2167

## 1 Part 1

### 1.1 Setup

This investigation will study the Schumann-Runge band of the  $^{16}\text{O}_2$  spectrum due to transitions from the  $X^3\Sigma_g^-$  ground electronic state (GS) to the  $B^3\Sigma_u^-$  excited state (ES). The potential energy (PE) curves for each state are Varshni potentials (equation 1), plotted in figure 1a.

$$V(x) = D_e \left(1 - \frac{r_e}{x} e^{-\beta(x^2 - r_e^2)}\right)^2 + T_e \quad (1)$$

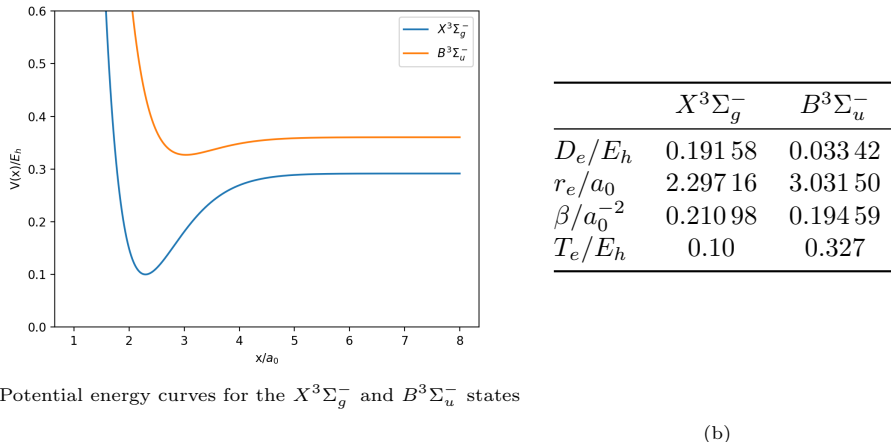


Figure 1: Potential energy curves and the values used to define each curve

Using the assumption that the ground vibrational state wavefunction for each electronic state is well approximated by a harmonic oscillator (HO) eigenfunction, we can calculate the force constant for each potential curve in the following way:

$$k_X = \frac{d^2V_X}{dx^2} \Big|_{x=r_e} = 2D_e^X \left( \frac{1}{r_e^X} + 2\beta^X r_e^X \right)^2 = 0.75597 \text{ Nm}^{-1} \quad (2)$$

$$k_B = \frac{d^2V_B}{dx^2} \Big|_{x=r_e} = 2D_e^X \left( \frac{1}{r_e^X} + 2\beta^X r_e^X \right)^2 = 0.15234 \text{ Nm}^{-1} \quad (3)$$

For a diatomic modelled by the harmonic oscillator, we use the reduced mass,  $\mu$ , to simplify the problem:

$$\mu = \frac{M_1 M_2}{M_1 + M_2} = \frac{16 * 16}{16 + 16} \frac{1}{5.486 * 10^{-4}} = 14582.6 \text{ m}_e \quad (4)$$

Figure 2 shows the harmonic approximations for the ground vibrational states of each PE curve, as well as the  $v = 0$  eigenfunctions calculated using the force constants and reduced mass.

Later, we will be using the transition dipole moment (TDM) (figure 3), which gives us the probability of transition between electronic states as a function of inter-atomic distance.

A crucial factor to consider is the size of the spatial domain (x grid of space points). This must be of adequate size in order to avoid the wavefunction interfering with itself at longer times, producing unwanted artefacts.

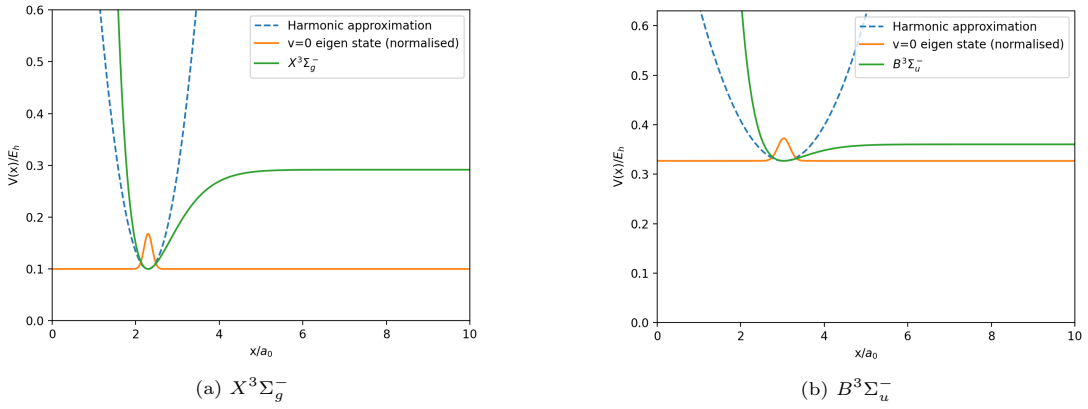


Figure 2: Plots showing the harmonic approximation for the ground vibrational state for each potential, and the ground vibrational eigenfunction for that  $v=0$  state. We are able to do this as at low vibrational levels the well is effectively symmetric.

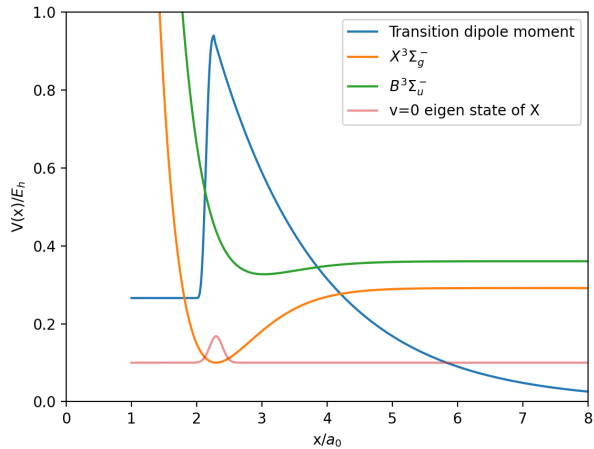


Figure 3: Transition dipole dependence on interatomic distance, overlayed ontop of the potential curve and the  $v=0$  eigenfunction of the GS potential. It can be seen the TDM peaks at the equilibrium bond distance, which makes sense as this this distance should have the greatest orbital overlap.

## 1.2 Time evolution along the Ground State potential

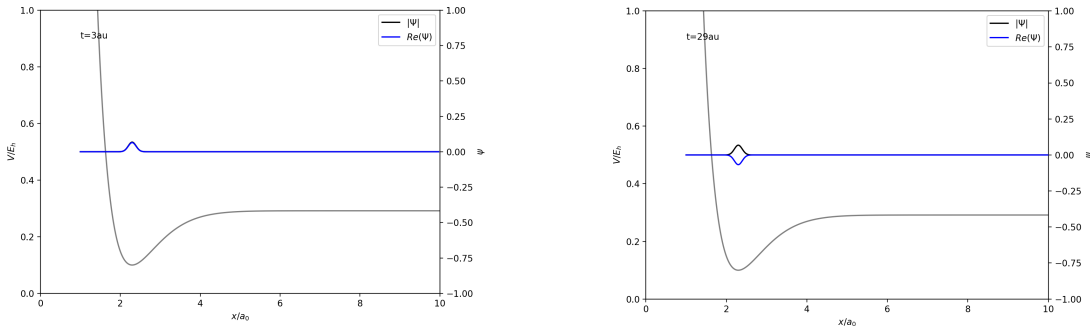
This first step does not aid calculation of the absorption spectrum directly, but is a check that everything is setup in the intended way. The GS Hamiltonian was applied in order to evolve the the  $v=0$  wavefunction of the GS potential in time, figure 4 showing snapshots in time. The autocorrelation function of the ground state was calculated using equation 5, producing figure 5a. The function is sinusoidal with maxima at 1 corresponding to complete overlap of the wavefunction at time  $t$  with the wavefunction at  $t=0$  (figure 4a) and minima at -1 corresponding to anti-overlap with the wavefunction at  $t=0$  (figure 4b).

$$\langle \psi(0) | \psi(t) \rangle = \int_{-\infty}^{\infty} \psi^*(x, 0) \psi(x, t) dx \quad (5)$$

$$S(\omega) = \mathcal{F}^{-1}[\langle\psi(0)|\psi(t)\rangle] = \frac{1}{\sqrt{2\pi}} \int_{-\infty}^{\infty} \langle\psi(0)|\psi(t)\rangle e^{i\omega t} dt \quad (6)$$

The power spectrum was then calculated with equation 6, producing figure 5b. In our case the integral is over our spatial domain (x grid of points). The power spectrum of a single eigenfunction is expected to have a single peak with energy equal to its eigenvalue, as it is composed of a single frequency oscillation. Here the peak value is  $0.104 E_h$ . We can calculate the expected value equation 7, but in our case the energy of the state involves an addition factor for the PE of the PE well minima, shown in equation 8. These values are equal to 3 s.f., confirming our setup and approximations used approximations produce accurate results.

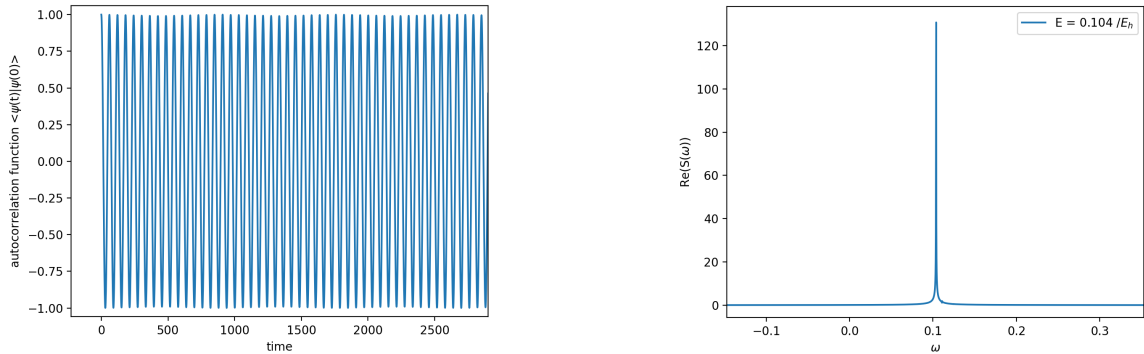
$$E_v = \left( v + \frac{1}{2} \right) \sqrt{\frac{k}{\mu}} \quad (7)$$



(a) Wavefunction showing complete overlap with  $t = 0$  wavefunction

(b) Wavefunction showing anti-overlap with  $t = 0$  wavefunction

Figure 4: Plots showing the  $v=0$  eigenfunction of the ground state PE curve oscillating in time. We see that the eigenfunction is stationary but its phase factor evolves in time, as expected for the harmonic oscillator.



(a) Autocorrelation function of the time evolution of the  $v=0$  eigenfunction along the GS PE curve. As the eigenfunction is stationary and trapped in the well, this signal does not decay.

(b) Power spectrum of the ground vibrational level of the ground state, obtained from the inverse Fourier transform of the autocorrelation function.

Figure 5: Autocorrelation function and power spectrum of GS time evolution on GS PE curve

$$E_{Tot} = E_0 + T_e = \left(0 + \frac{1}{2}\right) \sqrt{\frac{k}{\mu}} + T_e = 0.104 E_h \text{ (3.s.f.)} \quad (8)$$

### 1.3 Obtaining the Absorption spectrum - Excitation and propagation along the ES potential

The next step is to use the TDM function to excite the  $v=0$  wavefunction from the GS PE curve to the ES and evolve it in time by applying the ES Hamiltonian. The TDM,  $\mu$ , represents the interaction with light, therefore crucial for absorption spectrum calculation. We will be using time-dependant perturbation theory, which provides the framework for the interaction of a molecular system with light.

Figure 6 shows the propagation along the ES PE curve. It is seen that the excitation produces a bound state and an unbound state.<sup>1</sup> What this represents is the dissociation of the O<sub>2</sub> molecule, where a large part of the wavefunction dissociates in the form of a wavepacket, leaving behind a part as a bound state in the attractive potential well. It is seen that the unbound state is a wavepacket composed of continuous energies and therefore continuous momenta.

The autocorrelation function was calculated in figure 7a from equation 5. The shape is sinusoidal with an exponential decay. This is expected for a molecule where the majority of the wavefunction undergoes a dissociation as there will be very little overlap with the original wavefunction at large times. The timescales were investigated in table 2, and  $T_3$  was the largest, as expected, however, comparing to the timescale the propagation was looked at on, this value is not very large and the dissociation happens very quickly.  $T_3$  effects the peak width in the adsorption spectrum, where a slow decay yields sharp well defined peaks<sup>2</sup>. This could prove as a challenge to achieve a well resolved absorption spectrum. The first 200 time points of the autocorrelation function were omitted to investigate its long term behaviour in figure 7c. These recurrences in the autocorrelation function are due to the overlap of the bound state in the potential well with the wavefunction at  $t=0$ . Their amplitude is so small as the majority of the wavefunction has dissociated leaving only a small fraction of the wavefunction left behind.

The absorption spectrum (figure 8) was computed using equation 12, with the integral being over the

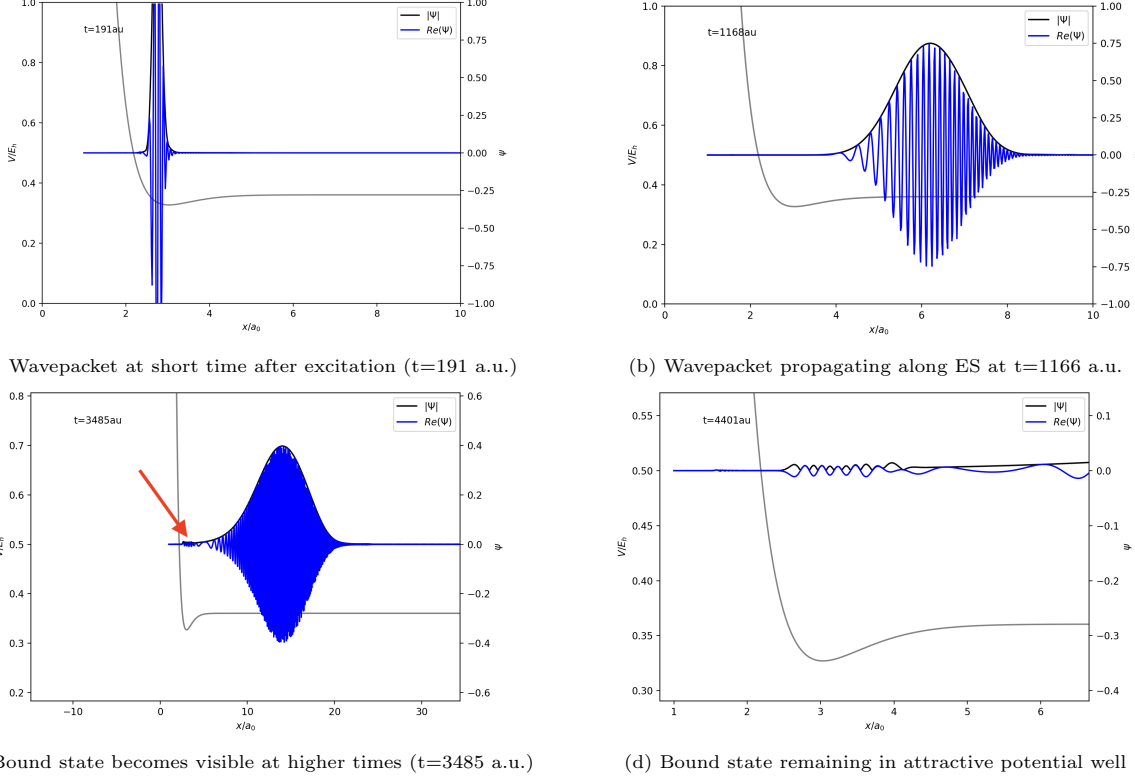


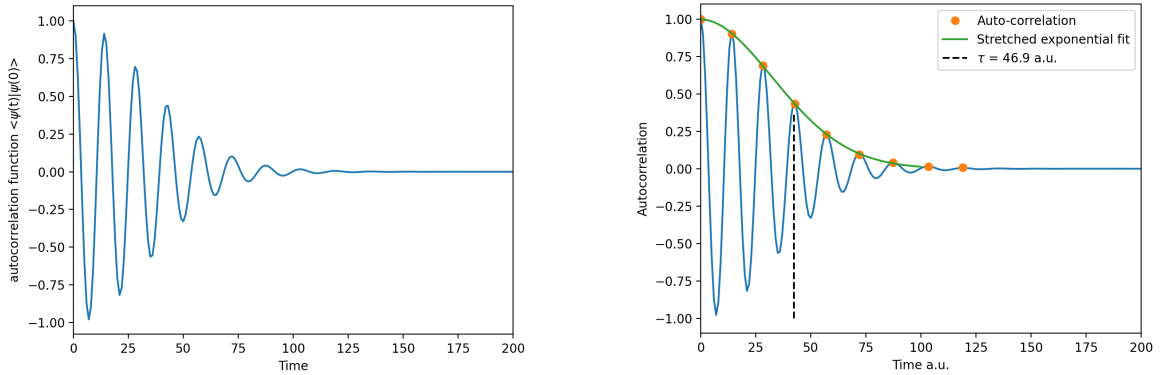
Figure 6: Plots showing snapshots of the propagation of the wavepacket formed by excitation along the ES potential. For the purpose of demonstrating its propagation, the wavefunction was not normalised in these images, however, the data used in the calculation of the autocorrelation function was for the normalised wavefunction. Propagation shows the characteristic broadening of the wavepacket over time due to the distribution of momenta - slow at the back, fast at the front.

Table 1: Timescales of the decay of the autocorrelation function where  $T_1$  is the short initial decay of the signal,  $T_2$  is the recurrence time between peaks and  $T_3$  is the recurrence decay.

	$T_1$	$T_2$	$T_3$
$\tau$ (a.u.)	2.001	14.021	46.922

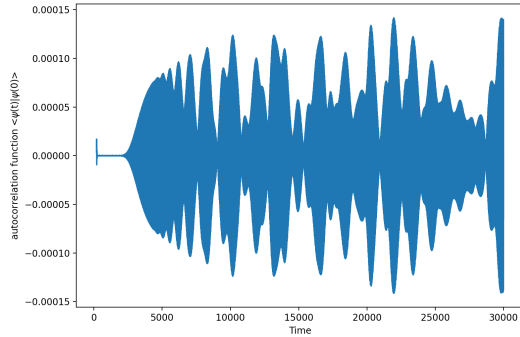
time domain ( $dt = 1$ ,  $nsteps = 30000$ ). This equation is a result of **time-dependant perturbation theory** and allows us to investigate the interaction of  $O_2$  with incident light of frequency  $\omega_I$  with the ground state eigenfunction of frequency  $E_i/\hbar$ <sup>3</sup>. Each peak in the absorption spectrum corresponds to a transition energy from  $v'=0$  on the GS potential ( $v'=0$  HO eigenfunction) to  $v''=v$  on the ES potential. The literature values for the Schumann–Runge bands of molecular oxygen occur between 176 and 192.6 nm<sup>4</sup>, matching extremely well with the absorption spectrum produced. All of these peaks correspond to transitions to bound states on the ES, which have discrete energy levels of uneven spacing.

$$\sigma(\omega_I) = \frac{2\pi\omega_I}{3\hbar c} \int_{-\infty}^{\infty} \langle \varphi(0) | \varphi(t) \rangle e^{i(E_i/\hbar + \omega_I)t} dt, \text{ where } \varphi = \hat{\mu}\psi \quad (9)$$



(a) Autocorrelation function of the wavefunction propagation along the excited state.  $T_1$  and  $T_2$  were easily extracted and are shown in table 2

(b) Fitting of the autocorrelation function to a stretched exponential decay in order to extract the long time decay constant  $T_3$ .



(c) Autocorrelation function excluding the first 200 time units to investigate its long term behaviour.

Figure 7: Autocorrelation function for propagation along the ES

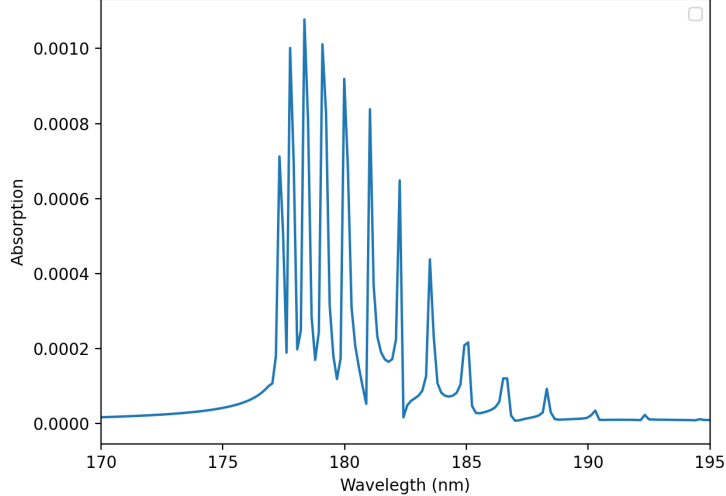


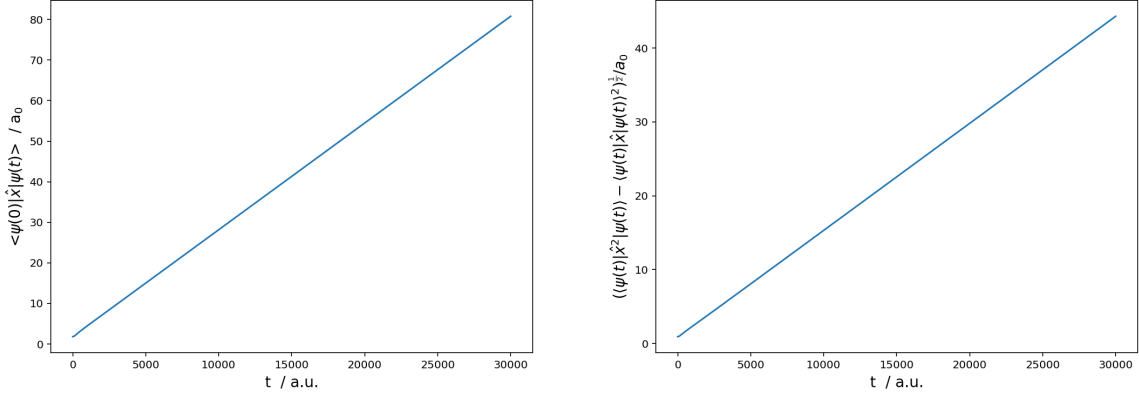
Figure 8: Absorption spectrum showing peaks in the range 177.6 - 192.5 nm. There are many peaks of different energies, suggesting excitation to many different vibrationally hot levels of the ES potential. The energies the absorption spectrum only correspond to the energy difference between the state its excited to and the GS (the relative energy), not the absolute energy.

#### 1.4 Mean and spread of ES propagation

$$\langle \hat{x} \rangle = \langle \psi(t) | \hat{x} | \psi(t) \rangle \quad (10)$$

$$\Delta x(t) = (\langle \psi(t) | \hat{x}^2 | \psi(t) \rangle - \langle \psi(t) | \hat{x} | \psi(t) \rangle)^{\frac{1}{2}} \quad (11)$$

Equations 10 and 11 were used to calculate the expectation and spread of the wavefunction's position at each time respectively. The expectation value for the position looks linear, which makes physical sense as the molecule is dissociating therefore as you increase the time, you expect the centre of the wavepacket to



(a) The expectation of the position value was calculated at every timestep in the propagation along the ES.  
(b) The spread of the position was calculated at every timestep in the propagation along the ES.

Figure 9: Mean and spread of the wavefunction's position over time.

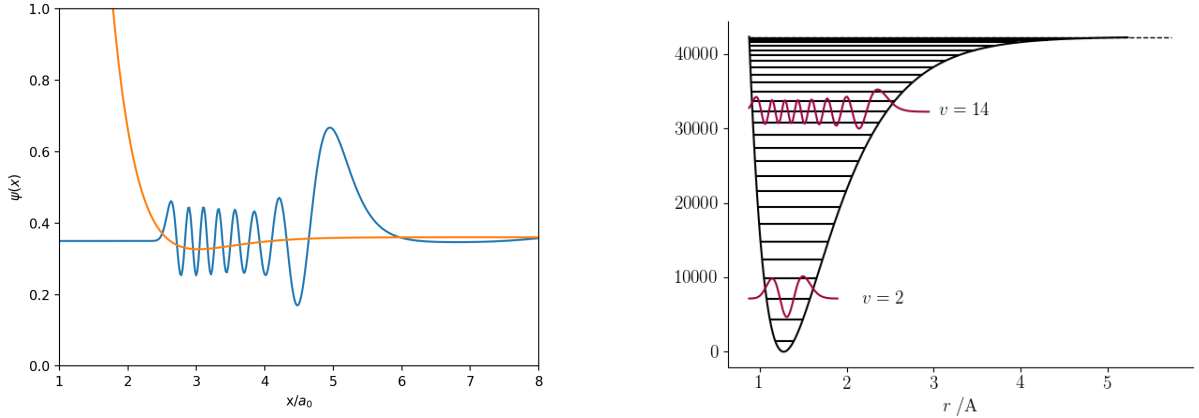
be at a higher x grid value. The spread of position is also linear due to the broadening of the wavepacket as time goes on due to differences in momentum values at the front compared to the back.

## 1.5 Eigenstates of the excited state curve

In order to find the resulting bound wavefunctions produced after excitation, the energies can be put into equation 13 as  $E_v^B$ . Figure 10a shows the eigenfunction when the eigenstate resulting from most intense vibronic transition is put into equation 13. The absolute energy of the state was found by:

$$E_v^B = E_0^X + E_{Transition}, \quad (12)$$

$$\int_{-\infty}^{\infty} e^{iE_v^B t} \varphi^B(x, t) dt = \sum_i c_i \int_{-\infty}^{\infty} e^{i(E_v^B - E_i^B)t} \Lambda_i^B(x) dt = 2\pi \sum_i c_i \delta(E_v^B - E_i^B) \Lambda_i^B(x) \propto \Lambda_v^B(x) \quad (13)$$



(a) Eigenfunction resulting from the most intense vibronic transition.

(b) Morse oscillator and its eigenfunctions.

Figure 10: Comparison of excited state eigenfunction to anharmonic oscillator eigenfunction.

The vibrational state of this eigenfunction can be found by counting the numbers of peaks and troughs and removing 1, which in this case we get  $v = 14$ . The eigenfunction of the excited state (for the most intense vibronic peak) closely resembles the  $v=14$  vibrational state for the anharmonic oscillator shown in figure 10b, which gives us reassurance that this is likely correct.

The Varshni potential can be compared to a more familiar anharmonic model, the Morse potential. The Schrodinger equation for the Morse oscillator is exactly solvable, giving vibrational eigenvalues:<sup>5</sup>

$$E_{v,Morse} = \omega \left( v + \frac{1}{2} \right) - \frac{\omega^2}{4D_e} \left( v + \frac{1}{2} \right)^2 \quad (14)$$

For  $v = 14$ :

$$E_{Tot} = E_{14, Morse} + T_e^B = 0.3574 \quad (15)$$

Whereas the value of  $E_v^B$  calculated from the absorption spectrum was 0.3589, suggesting a higher vibrational state that has been produced in figure 10a.

The intensity of the peaks in the absorption spectrum are related to the Frank Condon (FC) factor, which quantifies the overlap between the initial and final states:

$$FC = \langle \phi_f | \phi_i \rangle^2 \quad (16)$$

The  $v' = 0 \rightarrow v'' = 0$  has a FC factor many orders of magnitude smaller than the most intense vibronic

Table 2: FC factors. The value of the strongest vibronic peak should have the largest FC factor compared to the other transitions, and therefore the best overlap between  $\phi_i$  and  $\phi_f$ .

	$v' = 0 \rightarrow v'' = 14$	$v' = 0 \rightarrow v'' = 0$
FC factor	$7.730 \times 10^{-3}$	$9.769 \times 10^{-8}$

peak, which was expected as this peak is not observed in the absorption spectrum due to its small size due to poor overlap (the peak would be around 200 nm).

## 2 Part 2

### 2.1 Q1

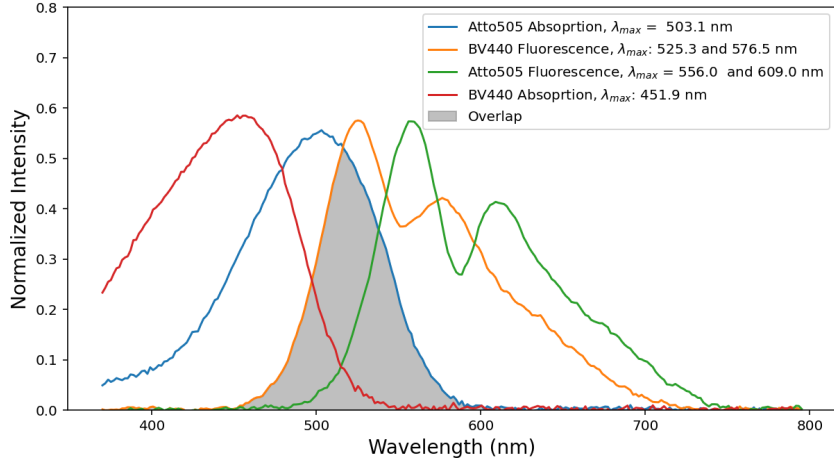


Figure 11: Absorption and fluorescence spectra for BV440 and Atto505 dyes, showing the overlap between BV440 fluorescence and Atto505 absorbance. The broadness of the fluorescence peak at higher wavelengths is likely emission to more vibrationally hot levels on  $S_0$  of BV440, but have lower intensities.

Figure 11 shows the absorption and fluorescence spectra for both the dyes. First considering BV440, the absorption peak corresponds to excitation from  $S_0^0 \rightarrow S_1^0$ , and the fluorescence peaks represent emission from  $S_1^0 \rightarrow S_1^1$  and  $S_1^1 \rightarrow S_0^0$ .<sup>6</sup> The  $S_1^0 \rightarrow S_1^1$  transition is red shifted from  $S_0^0 \rightarrow S_1^0$  due to the Stokes shift.<sup>7</sup> Even though this is a solid material, the Stokes shift is still possible, lowering the energy of the  $S_1^1$  level, leading to a lower energy gap and therefore a higher wavelength decay. A similar situation occurs for Atto505, however, it absorbs and fluoresces at higher wavelengths than BV440, meaning the energy gap between its  $S_0^0$  and  $S_1^0$  level is smaller than BV440's.

Significant overlap between the fluorescence of BV440 and the absorption of Atto505 is seen, which suggests an energy transfer process such as FRET is likely to be taking place, where BV440 is the donor and Atto505 is the acceptor. To understand if there is excitation to higher levels from  $S_1 \rightarrow S_N$  (photo-induced absorption (PIA)), we can look at the transient absorption (TA) spectrum in figure 13. This spectrum shows some negative regions at high wavelengths suggesting PIA is observed.

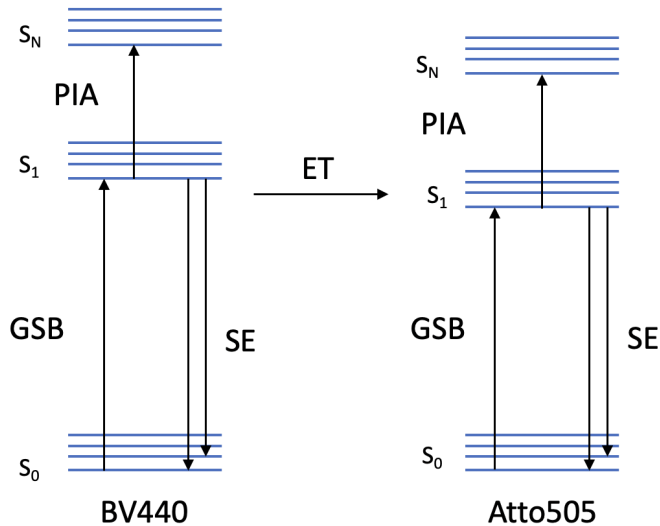


Figure 12: Jablonski diagram showing the key processes and excited states involved in the material. BV440: GSB (452 nm), SE (525, 577 nm). Atto505: GSB (503 nm), SE (556, 609 nm). As we know there is no phosphorescence, there will be no triplet formation and therefore triplet states are not included in the diagram.

The proposed Jablonski diagram is shown in figure 12, where the ground state bleach (GSB) corresponds

to the dyes respective absorptions, and stimulated emission (SE) corresponds to their respective emissions from the excited state to the ground state. Taking the energy of the  $S_0^0$  states of both dyes to be zero, the energy of  $S_1^0$  for BV440 is 451.9 nm = 2.74 eV, and the energy of  $S_1^0$  for Atto505 is 503.1 nm = 2.46 eV so slightly lower.

## 2.2 Q2

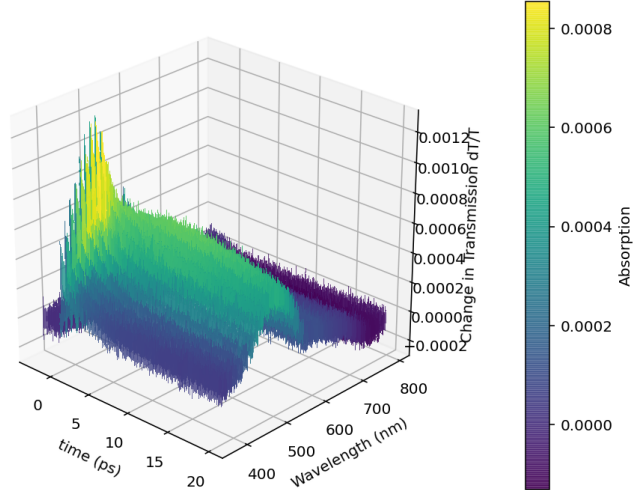


Figure 13: TA spectrum of the material.

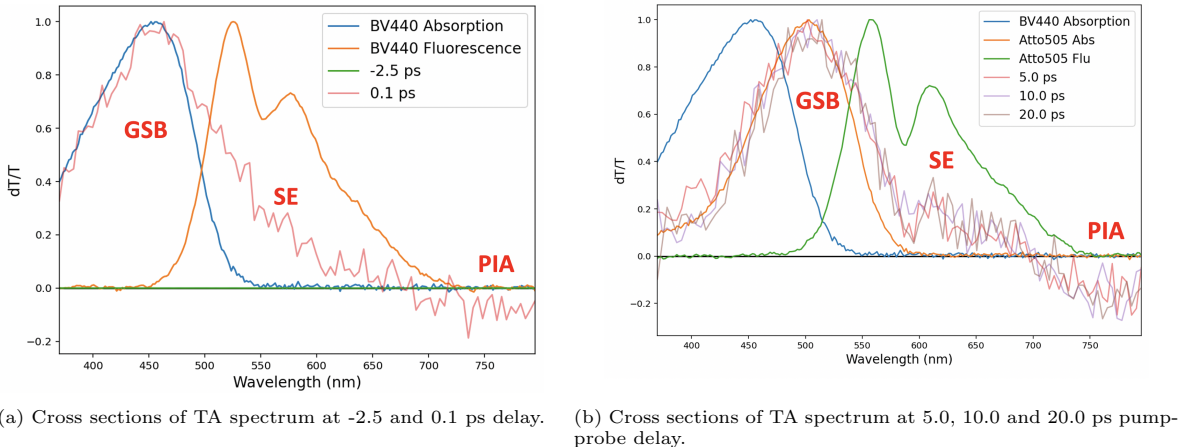


Figure 14: Time cross sections of TA spectrum. The pump-probe delay is how long the probe arrives after the pump pulse. This means that for a value of -2.5 ps the probe arrives 2.5 ps before the pump

Figure 14 shows cross sections of the TA spectrum at different pump-probe delays. Figure 14a first looks at delay = -2.5 ps where there is no excitation (probe before pump pulse) we get a flat line. The spectrum at 0.1 ps shows a ground state bleach (GSB) region which can be attributed to BV440 absorption due to the close alignment of the spectra.<sup>8</sup> This corresponds to populating the  $S_1^0$  state of BV440. At slightly higher wavelengths we have a simulated emission (SE) section, aligning with the emission from the  $S_1^0$  state of BV440. Some PIA is seen at higher wavelengths ( $S_1 \rightarrow S_N$ ). Figure 14b shows larger delays, which are all similar after 5.0 ps. At 5.0 ps the GSB's main contributor is now Atto505's absorption, occurring at a higher wavelength. There has been a decrease in intensity of BV440's contribution to the GSB, which must be due to a reduction in population of BV440's excited state due to energy transfer (ET) to Atto505, and also some PIA which is present at the higher wavelengths. As this peak has already decreased dramatically by 5.0 ps, it means the lifetime of the BV440  $S_1^0$  excited state must be under 5 ps. The SE section can be attributed to Atto505's emission, even with the higher wavelength bump matching up, giving us confidence of this hypothesis. Slightly more PIA is seen at these higher times, at a similar wavelength.<sup>8</sup>

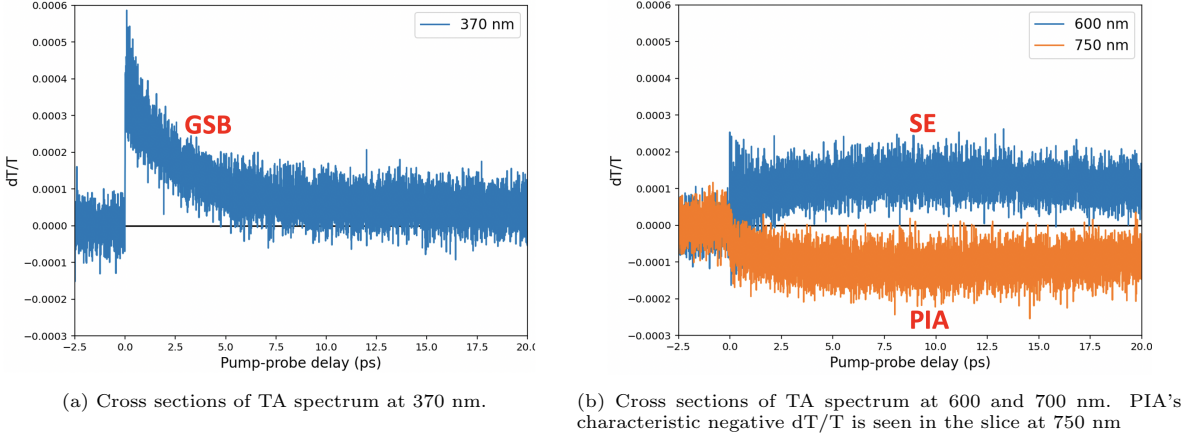


Figure 15: Kinetics of the TA spectrum from taking cross sections at different wavelengths. The locations of cross sections were guided by figure 15 in order to investigate the kinetics at the most relevant wavelengths possible.

Figure 15a shows the wavelength slice at 370 nm, which corresponds to the GSB due to BV440's absorption. We observe a decay in signal with a time constant  $\approx 2.3$  ps, agreeing with previous comments relating to figure 14. The cross sections in figure 15b correspond to SE and PIA. The SE curve shows the Atto505  $S_1^0$  state is seen to have a much longer lifetime than BV440  $S_1^0$  (GSB curve). PIA's  $S_N$  states also exhibit longer lifetimes.

### 2.3 Q3

The TA spectrum can be represented as the sum of all excited state contributions:

$$\Delta T(t, \lambda) = \sum_{l=1}^N \varepsilon^l(\lambda) c^l(t) \quad (17)$$

However, in experiment we use discrete  $t_i$  and  $\lambda_i$ , therefore the change in transmission can be represented as:

$$\Delta T_{ij} = \sum_{l=1}^N c_i^l \varepsilon_j^l, \quad (18)$$

where  $c_i^l$  is population of the excited state  $i$  at time  $t$  and  $\varepsilon_j^l$  is the spectrum of excited state  $i$ . With this equation in mind, we are able to use singular value decomposition (SVD) to extract the significant kinetics and spectra.<sup>9</sup>

SVD was performed to produce a singular values diagonal matrix, which is plotted in figure 16. We can see **only the first two states are significant**, which was confirmed mathematically. Figure 17 shows the kinetics and spectra of these two states.

At early times we assume only one state is populated: BV440. We know this as the system is excited with a 370 nm pump pulse, therefore comparing the dyes absorbances at 370 nm we can see BV440 absorbs much more efficiently than Atto505 at 370 nm, which absorbs minimally. Therefore we can assume at early times (e.g. 100 fs), the  $S_1^0$  excited state of BV440 is populated.

The coefficients for the states were altered until the two plots in figure 18 were achieved. For the combination  $c^{*1} = 0.5c^1 - c^2$  and  $\varepsilon^{*1} = 0.5\varepsilon^1 - \varepsilon^2$ , we can tell the spectrum corresponds to GSB for BV440 with a large absorption around 440 nm. The kinetics shows a fast decay of  $\tau = 2.31$  ps. The initial increase in population corresponds to the population of the  $S_1$  state via GSB, followed by the fast decay of this state via ET to Atto505's  $S_1$ . BV440's excited state therefore has a short life time. Now looking at the combination  $c^{*2} = 3.6c^1 - c^2$  and  $\varepsilon^{*2} = 3.6\varepsilon^1 - \varepsilon^2$ , the spectra corresponds to the GSB caused by Atto505 absorption. The corresponding kinetics resemble something interesting as Atto505 absorbs (GSB) but then the population increases further due to ET from the BV440 excited state. Atto505's excited state then decays slowly down to the ground state with a  $\tau = 39.46$  ps corresponding to SE from Atto's  $S_1 \rightarrow S_0$ . Energy transfer here has a much shorter characteristic time than the SE process. Figure 19 shows the resulting TA spectrum from recombination of the matrices with these new coefficients.

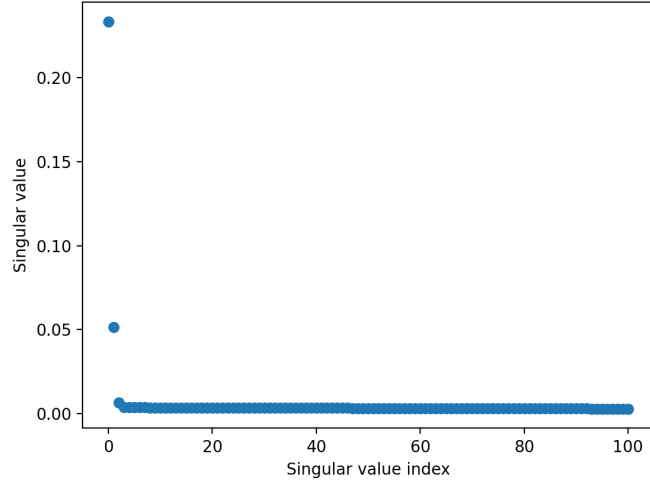


Figure 16: Plot of singular values as a visual aid to determine which are significant. A state was considered significant if:  $\sigma^l > 5 - 10\% \sigma^1$ , where  $\sigma^1$  is the weighting of the first state.

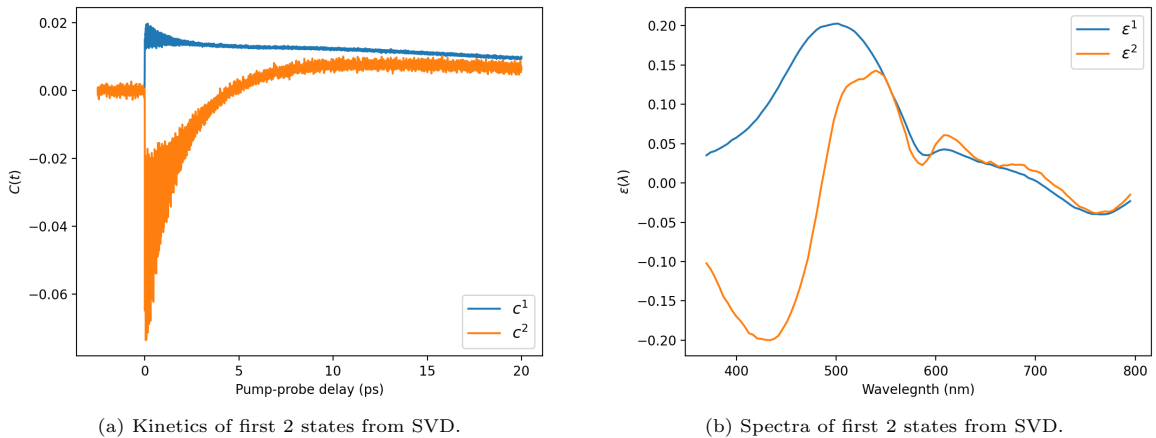
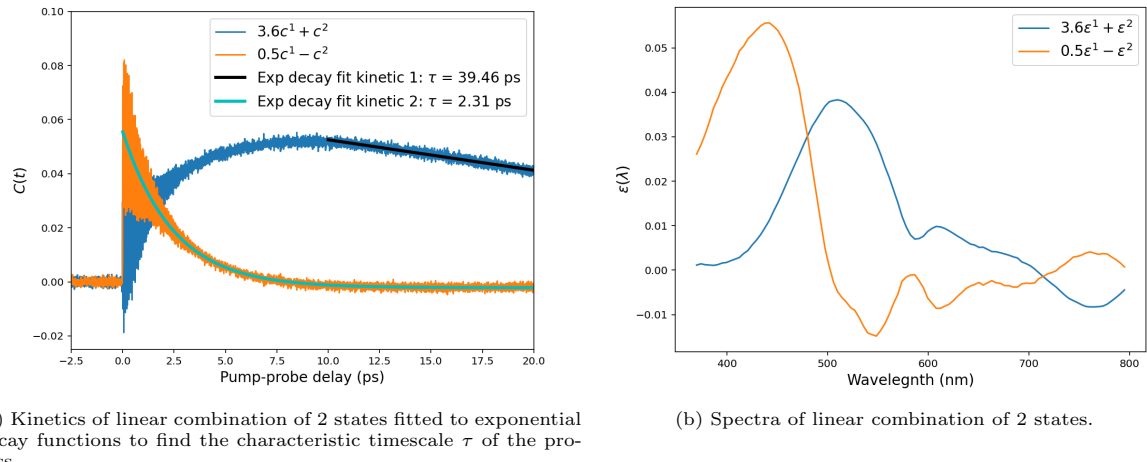


Figure 17: Kinetics and spectra of significant states found from SVD. The states by themselves do not have much physical meaning - we must experiment with linear combinations of states.



(a) Kinetics of linear combination of 2 states fitted to exponential decay functions to find the characteristic timescale  $\tau$  of the process.

(b) Spectra of linear combination of 2 states.

Figure 18: Kinetics and spectra linear combinations of states. For combination 1 kinetics the decay fitting was performed after the maximum. The larger value of  $\tau$  has been extrapolated and therefore is less accurate, but the important factor here is the relative sizes. A key assumption to help us choose linear combinations of spectra is that the population of a state cannot be negative (within fluctuation).

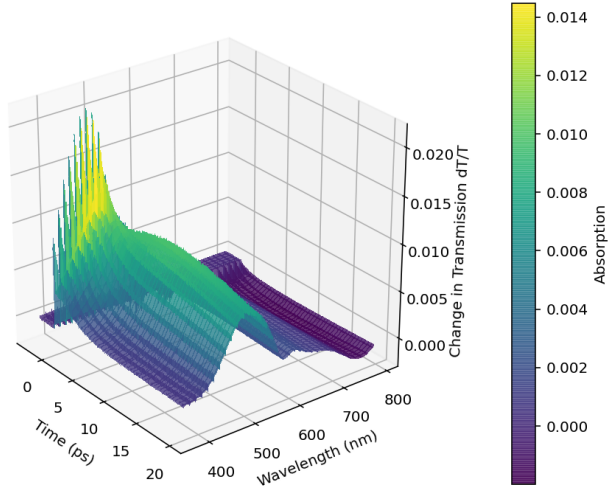


Figure 19: TA spectrum built from performing matrix multiplication on the kinetics, spectra and a diagonal matrix of our coefficients. The spectrum resembles the shape of the original TA spectra extremely well and has significantly reduced noise, giving us confidence in the chosen coefficients.

## 2.4 Q4

In order to identify the vibrational modes of BV440 and Atto505, impulsive Raman spectra must be plotted. Figure 20 shows the process of obtaining the Raman spectrum for the TA slice at 370 nm. From this we can see possibly two main peaks, but there is a large amount of noise. To help with this and also increase the accuracy of the extracted wavenumber, figure 21 takes the average over 100 wavelengths in the range of the TA spectrum to produce a very well resolved result. The plot shows **two vibrational modes at  $899.1$  and  $1131.9\text{ cm}^{-1}$** , which will be investigated further. Producing 3D and contour plots of the wavelength spectrum in figure 22 allows us to do this.<sup>10</sup> Two vibrational modes are observed at  $899.1$  and  $1131.9\text{ cm}^{-1}$ , with the higher energy mode ( $1131.9\text{ cm}^{-1}$ ) corresponding to the  $S_1$  state and the lower energy mode corresponding to  $S_0$ . GSB of BV440 is seen in the lower wavelength range of around 400-500 nm, and the higher wavelengths 500-600 nm is likely GSB of Atto505.

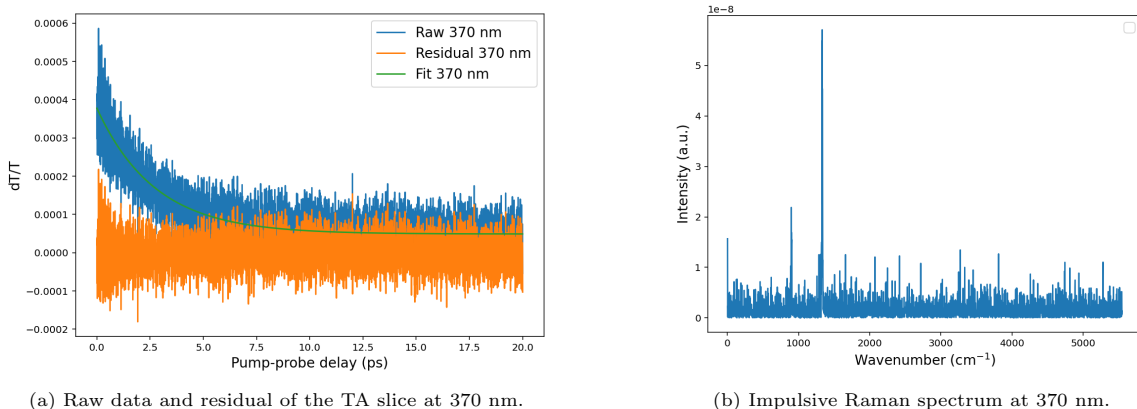


Figure 20: The residual is calculated from the difference between the raw data (TA slice) and the exponential decay fit. The impulsive Raman spectrum was then achieved by Fourier transform of the residual.

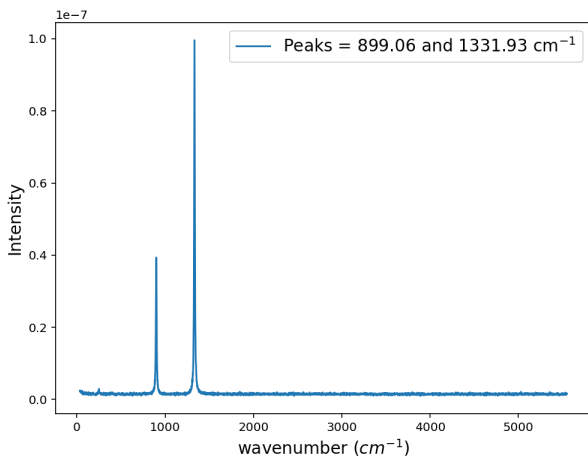


Figure 21: Averaged Impulsive Raman spectrum. The fit and residual were calculated for 100 points over the wavelength range. A fourier transform was then performed and the average taken.

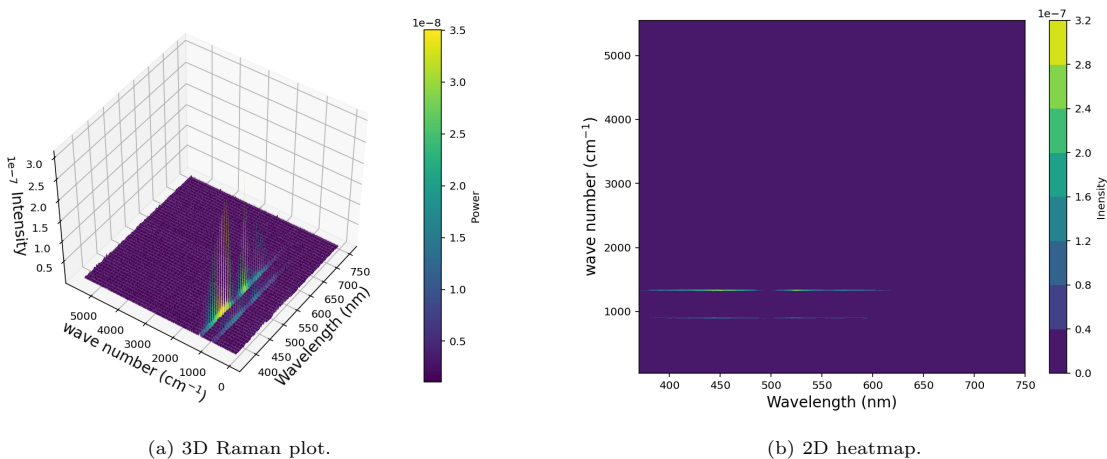


Figure 22: Impulsive Raman spectrum over wavelength range of TA spectrum in order to separate different coherences. These plots allow relation of the wavenumber and intensity of peaks in the Raman spectrum in figure 21 to a wavelength.

## References

- [1] G. C. Schatz and M. A. Ratner, *Quantum mechanics in chemistry*, Courier Corporation, 2002.
- [2] E. J. Heller, *Accounts of Chemical Research*, 1981, **14**, 368–375.
- [3] D. J. Tannor, *Introduction to quantum mechanics: a time-dependent perspective*, 2007.
- [4] G. P. Brasseur, S. Solomon *et al.*, *Springer Earth and Environmental Science eBooks 2005 English/International*, 2005.
- [5] R. Román-Ancheyta and J. Récamier, in *Advances in Quantum Chemistry*, Elsevier, 2015, vol. 71, pp. 299–322.
- [6] A. Bose, I. Thomas and E. Abraham, *International journal of advances in pharmaceutical analysis*, 2018, **8**, 1–8.
- [7] A. Iida and S. Yamaguchi, *Chemical communications*, 2009, 3002–3004.
- [8] R. Berera, R. van Grondelle and J. T. Kennis, *Photosynthesis research*, 2009, **101**, 105–118.
- [9] M. Schmidt, S. Rajagopal, Z. Ren and K. Moffat, *Biophysical journal*, 2003, **84**, 2112–2129.
- [10] N. Petkov, A. Ivanova, A. A. Trifonov, I. C. Buchvarov and S. S. Stanimirov, *Physical Chemistry Chemical Physics*, 2021, **23**, 20989–21000.